THE ASTROPHYSICAL JOURNAL, 557:1007–1020, 2001 August 20

IONIZATION PROPERTIES AND ELEMENTAL ABUNDANCES IN DAMPED Lyα SYSTEMS

GIOVANNI VLADILO, MIRIAM CENTURIÓN, AND PIERCARLO BONIFACIO
Osservatorio Astronomico di Trieste, Via G.B. Tiepolo 11, 34131 Trieste, Italy

AND

J. CHRISTOPHER HOWK
Department of Physics and Astronomy, Johns Hopkins University, 3400 North Charles Street, Baltimore, MD 21218
Received 2000 October 30; accepted 2001 April 16

ABSTRACT

We analyze extant data of Al^{+2}, Al^{+}, and other low ions with the aim of studying the ionization properties of damped Lyα systems (DLAs) from the analysis of the ratio $R(Al^{+2}/Al^{+}) \equiv N(Al^{+2})/N(Al^{+})$. We find the good correlations log $N(Al^{+})$–log $N(Si^{+})$ and log $N(Al^{+})$–log $N(Fe^{+})$ that we use to indirectly estimate $N(Al^{+})$ from $N(Si^{+})$ and/or $N(Fe^{+})$ measurements. In this way, we determine the ratio $R(Al^{+2}/Al^{+})$ for a sample of 20 DLAs. Contrary to common belief, the ratio can attain relatively high values (up to 0.6), suggesting that the gas of the intermediate ionization state plays an important role in DLAs. On the other hand, the lack of any trend between abundance ratios, such as Si/H and Si/Fe and $R(Al^{+2}/Al^{+})$ indicates that abundances are not severely influenced by ionization effects. We find a log $R(Al^{+2}/Al^{+})$–log $N(H^{0})$ anticorrelation that we use in conjunction with idealized photoionization equilibrium calculations to constrain the ionization properties and to predict ionization corrections in DLAs. We consider two possible origins for the species of the low- and intermediate-ionization state: (1) neutral regions devoid of Al^{+2} and/or (2) partially ionized, Al^{+2}-bearing regions. The log $R(Al^{+2}/Al^{+})$–log $N(H^{0})$ anticorrelation can be naturally explained in terms of a two-region model with a soft, stellar-type ionizing radiation field. We present abundance ionization corrections for 14 elements of astrophysical interest derived with different types of ionizing spectra. For most of these elements, the corrections are generally below measurements errors, which is contrary to the predictions of recent models presented in the literature. We briefly discuss the potential effects of inaccuracies in the Al recombination rates used in the photoionization calculations.

Subject headings: galaxies: abundances — intergalactic medium — quasars: absorption lines — radiative transfer

1. INTRODUCTION

The quasi-stellar object (QSO) absorption systems with hydrogen column densities $N(H^{0}) > 2 \times 10^{20}$ cm^{-2}—called damped Lyα systems (DLAs)—are believed to originate in intervening galaxies or protogalaxies located at cosmological distances (Wolfe et al. 1995). High-resolution spectroscopy of DLAs is a fundamental tool for probing the chemical and physical properties of the associated high-z galaxies and, more generally, of the high-redshift universe. In particular, abundance studies have been performed in order to probe the nature of DLA galaxies and to cast light on the early stages of galactic evolution (Lu, Sargent, & Barlow 1996; Pettini et al. 1997; Prochaska & Wolfe 1999; Molaro et al. 2000). In abundance studies it is important to take into account both dust depletion and ionization effects before deriving conclusions on the nucleosynthetic processes at work in DLA galaxies. The effects of dust depletion have been investigated by several research groups (Lauroesch et al. 1996; Kulkarni, Fall, & Truran 1997; Vladilo 1998, hereafter Paper I; Savaglio, Panagia, & Stiavelli 2000). All these studies indicate that dust corrections can have a significant impact on our understanding of the chemical history of DLAs. In order to cast light on the intrinsic abundance trends, some authors have analyzed DLAs with a modest or negligible dust content (Pettini et al. 2000; Molaro et al. 2000) or elements that are essentially unaffected by dust depletions (Centurión et al. 1998).

In the present work we investigate the effects of ionization on the observed abundances. These effects are generally neglected because the abundances are derived from dominant ionization states of the elements of interest. It is well known from Galactic interstellar studies that the dominant ionization state in H^{0} regions is the neutral one for elements with the first ionization potential IP > 13.6 eV (e.g., O^{0}, N^{0}) and the singly ionized one for elements with the first IP < 13.6 eV and the second IP > 13.6 eV (e.g., C^{+}, Mg^{+}, Al^{+}, Si^{+}, S^{+}, Cr^{+}, Mn^{+}, Fe^{+}, and Zn^{+}). The reason for this is that the bulk of the H^{0} gas is self-shielded from $h\nu > 13.6$ eV photons but transparent to $h\nu < 13.6$ eV photons. The first studies of ionization balance in DLAs have indicated that ionization corrections are negligible for the low ions used in abundance determinations (Viegas 1995; Lu et al. 1995; Prochaska & Wolfe 1996). However, the presence of Al^{+2} in DLAs suggests that ionization corrections may be important. From the aluminum ionization potentials—$IP(Al^{0}) = 5.99$ and $IP(Al^{+}) = 18.83$ eV—one expects Al^{+} to be dominant and Al^{+2} to be essentially absent in H^{0} regions. The observations indicate that Al^{+2} is present in DLAs at the same radial velocity as low ions but at a different radial velocity than high ions such as C^{+3} and Si^{+3} (Lu et al. 1996; Prochaska & Wolfe 1999; Wolfe & Prochaska 2000). Clearly, Al^{+2} is a tracer of the moderately ionized gas associated with the neutral phase, and the study of the Al^{+2}/Al^{+} ratio must bear important information on the effects of ionization on the derived abundances.

In a previous work we have performed detailed ionization calculations relevant to the ionized layer directly exposed to the ionizing radiation field (Howk & Sembach 1999, hereafter Paper II). In that work the photoionization calculations have been stopped at the point at which the

local ionization fraction of neutral hydrogen climbs above 10%. In the present work we first study the Al^{+2}/Al^{+} ratio from the observational point of view, and we then perform photoionization calculations aimed at modeling this ratio. Rather than analyzing individual absorbers, we study the general behavior of the Al^{+2}/Al^{+} ratio in a relatively large sample of DLAs. In our computations we consider the possibility that the line of sight can intersect both the neutral gas and partially ionized gas. At variance with Paper II, we also perform photoionization calculations that are stopped at fixed $N(H^0)$-values.

2. ANALYSIS OF OBSERVATIONAL DATA

In Table 1 we present a compilation of aluminum column densities in DLAs collected from the literature. References to the original works are reported in column (6). Only measurements performed on high-resolution spectra obtained with 10 m–class telescopes have been included in the list. Most of the data have been obtained with the Keck High Resolution Echelle Spectrograph (HIRES) and analyzed by only a few authors. The collected data set is therefore quite homogeneous from the observational point of view. Nevertheless, we paid special attention on the reliability of the published column densities. In particular, we revised the available data for rejecting cases suspected to be affected by saturation or by telluric contamination. In addition, we investigated the velocity distribution of the absorption profiles. In fact, the comparison of the column densities of Al^{+}, Al^{+2}, and other low ions that we perform here makes sense only if these ions have similar velocity profiles, suggesting that they are physically related.

The Al^{+} column densities are derived from the transition at $\lambda_{lab}167.0$ nm, which is often saturated. In fact, only lower limits are reported in the literature for a large fraction of cases. We have, in addition, found three more cases of suspected saturation from a revision of the absorption pro-

TABLE 1

Al^{+} AND Al^{+2} COLUMN DENSITIES IN DLA SYSTEMS

QSO (1)	z_{abs} (2)	log N_{HI} (3)	log $N(Al^{+2})$ (4)	log $N(Al^{+})$ (5)	References (6)	log $N(Al^{+})^{a}_{pred}$ (7)	log $[N(Al^{+2})]/[N(Al^{+})]$ (8)
0000−263.....	3.3901	21.41 ± 0.08	12.54 ± 0.10[b]	>13.15	1	13.66 ± 0.17	−1.12 ± 0.20
0100+130.....	2.3090	21.40 ± 0.05	12.72 ± 0.03	...	2	14.17 ± 0.25	−1.45 ± 0.25
0149+33	2.1400	20.50 ± 0.10	12.56 ± 0.04	12.94 ± 0.10	2	13.14 ± 0.18	−0.38 ± 0.11
0201+365.....	2.4620	20.38 ± 0.04	13.61 ± 0.01	...	3	14.14 ± 0.24	−0.53 ± 0.17
0216+080.....	1.7688	20.00 ± 0.18	13.20 ± 0.07	...	1	13.46 ± 0.20	−0.26 ± 0.21
0216+080.....	2.2931	20.45 ± 0.16	13.74 ± 0.02	>13.88	1	14.03 ± 0.22	−0.29 ± 0.22
0307−4945	4.466	20.67 ± 0.09	...	13.36 ± 0.06	4	13.28 ± 0.17	...
0458−02	2.0400	21.65 ± 0.09	13.34 ± 0.02	>13.72	2	...	...
0528−2505	2.1410	20.70 ± 0.08	12.77 ± 0.08	>13.46	1	13.84 ± 0.19	−1.07 ± 0.20
0528−2505	2.8110	21.20 ± 0.10	>14.07	>14.20	1	...	...
0841+129.....	2.3745	20.95 ± 0.09	12.60 ± 0.10[c]	>13.26	2	13.82 ± 0.18	−1.21 ± 0.21
0841+129.....	2.4764	20.78 ± 0.10	12.63 ± 0.04	>13.19[d]	2	...	...
0951−0450	3.8570	20.60 ± 0.10	...	13.30 ± 0.02	2	13.22 ± 0.17	...
1104−1805	1.6616	20.85 ± 0.01	13.06 ± 0.02	>13.43[d,e]	5	13.96 ± 0.21	−0.90 ± 0.21
1215+33	1.9990	20.95 ± 0.07	12.78 ± 0.02	>13.36	2	13.61 ± 0.17	−0.84 ± 0.17
1331+170.....	1.7764	21.18 ± 0.04	12.97 ± 0.01[f]	>13.57	2	13.86 ± 0.19	−0.88 ± 0.19
1346−0322	3.7360	20.70 ± 0.10	...	12.55 ± 0.03	2	12.52 ± 0.17	...
1425+603.....	2.8268	20.30 ± 0.04	...	>13.55	1	...	...
1795+75	2.6250	20.80 ± 0.10	13.62 ± 0.04[f]	...	2	14.11 ± 0.24	−0.49 ± 0.24
1946+765.....	1.7382	...	12.70 ± 0.04	...	1	13.33 ± 0.17	−0.63 ± 0.18
1946+765.....	2.8443	20.27 ± 0.06	<12.09	12.26 ± 0.03	1, 6	12.19 ± 0.17	<−0.17
2206−199A.....	1.9200	20.65 ± 0.10	13.88 ± 0.01[f]	...	7	14.39 ± 0.28	−0.51 ± 0.28
2206−199A.....	2.0760	20.43 ± 0.10	...	12.18 ± 0.01	7	12.32 ± 0.17	...
2230+025.....	1.8642	20.85 ± 0.08	13.60 ± 0.01[f]	>14.02	2	14.24 ± 0.26	−0.64 ± 0.26
2231−0015	2.0662	20.56 ± 0.10	13.14 ± 0.03[c]	...	2	13.83 ± 0.19	−0.69 ± 0.19
2237−0607	4.0803	20.52 ± 0.11	...	12.85 ± 0.02	1	12.84 ± 0.17	...
2348−147.....	2.2790	20.56 ± 0.08	11.95 ± 0.08[g]	12.65 ± 0.01	2	12.79 ± 0.17	−0.70 ± 0.08
2359−0216	2.0950	20.70 ± 0.10	12.88 ± 0.05[g]	>13.66[d]	2	13.99 ± 0.23	−1.11 ± 0.24
2359−0216	2.1540	20.30 ± 0.10	12.96 ± 0.02	13.17 ± 0.02	2	12.88 ± 0.20	−0.20 ± 0.03

[a] Value estimated from $N(Si^{+})$ and from the linear relation shown in Fig. 1. The error bar is obtained from error propagation of the $N(Si^{+})$ error and of the linear regression error. The latter is estimated by taking into account the dispersion of the linear regression σ and the errors σ_m and σ_q given in the third row of Table 2.

[b] Value determined from the UVES spectrum presented by Molaro et al. 2000. Only the Al^{+2} line at 186.2 nm has been used. The line at 185.4 nm is affected by telluric contamination.

[d] The published value is treated as a lower limit since the line is saturated in a substantial part of the profile.

[c] Mean value of the lines at 185.4 and 186.2 nm.

[e] The profile fitting result given by the authors is not reliable owing to the strong saturation of the line; we adopt as a lower limit the result of the optical depth analysis.

[f] The Al^{+2} absorption profile shows one or more features that are not seen or are much weaker in the absorption profiles of low ions; the equivalent width of such features is significantly smaller than that of the bulk of the absorption seen also in low ions.

[g] The column density refers only to the Al^{+2} absorption profile in the radial velocity range where the bulk of low ions is observed; a high-velocity Al^{+2} absorption component is also present, but its column density is not reported here.

REFERENCES.—(1) Lu et al. 1996; (2) Prochaska & Wolfe 1999; (3) Prochaska & Wolfe 1996; (4) Dessauges-Zavadsky et al. 2001; (5) Lopez et al. 1999; (6) Lu et al. 1995; (7) Prochaska & Wolfe 1997.

files. We also treat these three cases as lower limits even if they are quoted as real measurements in the original works (see footnote d in the table).

The Al^{+2} column densities are derived from the transitions at λ_{lab}185.4 and λ_{lab}186.2 nm, which are not affected by saturation effects. Our reanalysis of the velocity profiles confirms that Al^{+2} has, in general, the same velocity distribution as the low ions (Wolfe & Prochaska 2000). However, we found some exceptions, which are marked with the explanatory footnotes f and g in Table 1. Typically, we found evidence for an additional Al^{+2} absorption component displaced from the zero-velocity component seen in Al^{+} and/or other low ions. In most of these cases, the equivalent width of this extra absorption is negligible compared to the total Al^{+2} absorption. The bulk of Al^{+2} originates in the same velocity range as Al^{+} and the other low ions.

For the absorber at $z = 3.3901$ toward QSO 0000−263, we found evidence for telluric contamination of the Al^{+2} 185.4 nm profile from the analysis of a newly obtained spectrum of this target by means of the Ultraviolet-Visual Echelle Spectrograph (UVES) at the Very Large Telescope (Molaro et al. 2000). In Table 1 we report the column density obtained from the analysis of the 186.2 nm line, which is unaffected by contamination. Careful inspection of the full set of profiles in the other DLAs of Table 1 does not reveal evidence for telluric contamination since the profiles of the two lines of the doublet are always similar when they are both available (in almost all cases).

2.1. *Column Density Correlation Analysis*

While Al^{+} and other singly ionized species with IP < 13.6 eV can be present in the inner parts of H^0 regions, the production of Al^{+2} requires photons with $h\nu > 18.8$ eV, which cannot as easily penetrate large H^0 column densities. A careful analysis should therefore reveal a different behavior between Al^{+2} and singly ionized species. Since the radial velocity analysis does not show evidence for a distinct behavior, we investigated the column density behavior of such species. For two species that are present in roughly constant proportions in the same region, we expect to find a linear correlation with a slope of unity between their logarithmic column densities. The identification of such a correlation would support a common origin of the different species. The lack of such a correlation could be ascribed to differences in the abundance/depletions patterns or to differences in the ionization properties. By analyzing ions of the same elements, such as Al^{+2} and Al^{+}, there can be no differences in the intrinsic abundances. Studying such ions, therefore, gives information on the ionization state of the gas, and a slope differing from unity would indicate that ionization properties do affect the observed column densities. Unfortunately, only a modest number of simultaneous determinations of Al^{+} and Al^{+2} in DLAs are currently known (Table 1). To bypass this limitation, we compared the column densities of both Al^{+} and Al^{+2} ions with those of Fe^{+} and Si^{+}, for which a large number of measurements are instead available. In practice, we performed a linear regression analysis of the column densities of each possible combination of pairs of the species Al^{+}, Al^{+2}, Si^{+}, and Fe^{+}. The results are summarized in Table 2, where we give for each pair the number of data points available n, the correlation coefficient r, the slope m, and the intercept q resulting from the linear regression. In Figure 1 we show the results for Al^{+} and Si^{+}.

TABLE 2

LINEAR REGRESSION ANALYSIS OF LOGARITHMIC COLUMN DENSITIES IN DLA SYSTEMS

Ions	n	r	σ	$m \pm \sigma_m$	$q \pm \sigma_q$
Si^{+} vs. Fe^{+}	30	0.96	0.17	0.99 ± 0.06	0.64 ± 0.82
Al^{+} vs. Fe^{+}	8	0.91	0.20	1.20 ± 0.22	-3.73 ± 3.10
Al^{+} vs. Si^{+}	9	0.94	0.16	1.05 ± 0.15	-2.20 ± 2.11
Al^{+2} vs. Fe^{+}	20	0.51	0.37	0.46 ± 0.18	6.25 ± 2.70
Al^{+2} vs. Si^{+}	17	0.74	0.35	0.83 ± 0.19	0.45 ± 2.94

One can see from Table 2 that singly ionized species, including Al^{+}, are well correlated with each other and have a slope of unity within the errors.[1] This fact, together with the similarity of the velocity profiles, suggests that all these species originate in the same region. On the other hand, pairs of species including Al^{+2} show a modest correlation coefficient and a slope significantly lower than 1. In addition, such pairs have larger dispersions than the corresponding pairs with Al^{+}. For instance, $\sigma(Al^{+2}, Si^{+}) \simeq 2\,\sigma(Al^{+}, Si^{+})$. This distinct behavior of Al^{+2} cannot be attributed to differences in the abundances or dust depletion properties of Al, Fe, and Si. If such effects were important, they would also tend to cancel the correlations between Al^{+} and Fe^{+} and between Al^{+} and Si^{+}, which are instead clearly detected. Since the distinct behavior of Al^{+2} is not due to intrinsic variations of the abundances/depletions, it must be due to the ionization properties of DLA clouds. This observational result can be interpreted in the following two ways:

1. The Al^{+2} originates in the same H^0 region as the bulk of the low-ionization lines. The local value of the Al^{+2}/Al^{+} ratio varies among DLA clouds.

2. The Al^{+2} originates in a region distinct from but physically related to the H^0 region in which the bulk of the

[1] Chemical evolution and dust effects are hidden within the dispersion of the correlations. At first sight, it is surprising that such effects do not introduce a large scatter. However it is possible to show that changes in the metallicity level and dust content tend to compensate each other since relative abundances scale with the dust-to-metals ratio (eq. [17] in Paper I) and at the same time metallicity and dust content are correlated in DLAs (Fig. 2 in Paper I). On the other hand, the intrinsic spread of relative abundances due to chemical evolution may be modest owing to the relatively limited range of look-back time explored in DLAs (most absorbers are found at $z \simeq 2.5$).

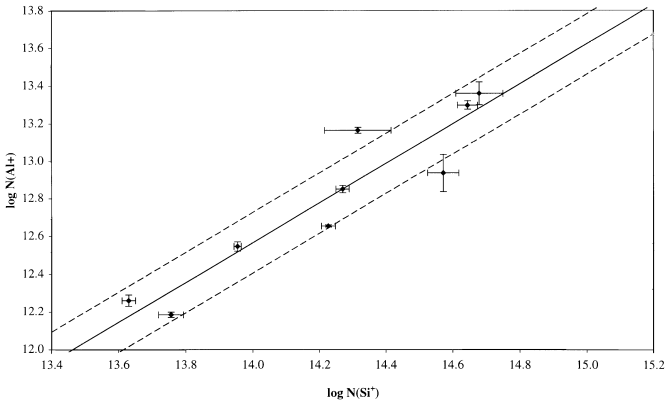

FIG. 1.—Comparison of Al^{+} and Si^{+} column densities in DLAs. *Solid line*: Linear regression of the data points. *Dashed lines*: $\pm 1\,\sigma$ dispersion of the linear regression.

singly ionized species reside. The relative column density contribution from the two regions varies among DLA clouds.

Studies of the ionization properties of DLAs usually consider only the first of the two possibilities. Here we will also consider the second one. A separate Al^{+2} region may, in fact, exist if the photons with $h\nu > 18.8$ eV required for producing Al^{+2} are not available in the self-shielded parts of the H^0 region. Since the velocity structures of Al^{+2} and of low ions are generally similar, the Al^{+2} and H^0 regions must be physically connected. A cloud structure consisting of a partially ionized Al^{+2}-bearing interface bordering an H^0 region opaque to $h\nu > 13.6$ eV photons satisfies the above requirements.

2.2. *The* Al^{+2}/Al^{+} *Ratio in DLAs*

The Al^{+2}/Al^{+} ratio can be used to constrain the ionization conditions and/or the ionization structure of DLAs. From the observational point of view, we are able to measure the column density ratio $R(Al^{+2}/Al^{+}) \equiv N(Al^{+2})/N(Al^{+})$, which gives information integrated along the line of sight. Direct measurements of $R(Al^{+2}/Al^{+})$ are currently possible only in a few cases, mainly because reliable Al^{+} measurements are quite rare (Table 1). For this reason, we take advantage of the existence of the log $N(Al^{+})$–log $N(Fe^{+})$ and log $N(Al^{+})$–log $N(Si^{+})$ correlations to estimate indirectly $N(Al^{+})$ from Fe^{+} and Si^{+} measurements. The indirect determinations based on Si^{+} measurements are displayed in column (7) of Table 1. References to the original Si^{+} measurements are the same given in column (6). These indirect estimates of $N(Al^{+})$ yield results consistent with all the available Al^{+} data (i.e., nine determinations and also nine lower limits). Similar results are obtained when Fe^{+} is used to track Al^{+} (see more details in § 2.4). Because the correlation with $N(Si^{+})$ has a lower dispersion, lower slope error, and lower intercept error than the correlation with $N(Fe^{+})$ (Table 2), we use the Si^{+}-based results given in Table 1 in the rest of the paper unless otherwise specified.

In the last column of Table 1, we list the values of the aluminum ionization ratio in DLAs obtained by using indirect and, when possible, direct measurements of Al^{+}. The ionization ratio shows a spread of more than 1 order of magnitude, with values ranging from $R(Al^{+2}/Al^{+}) \simeq 0.03$ up to $\simeq 0.6$ and a median value $\simeq 0.2$. Values of $R(Al^{+2}/Al^{+})$ as high as 0.6 are also detected in the subsample for which $N(Al^{+})$ is measured directly. The presence of high fractions of doubly ionized aluminum suggests that Al^{+} is not the only ionization state of aluminum present in significant amounts in DLAs. However, it is unsafe to use $R(Al^{+2}/Al^{+})$, which is a quantity integrated along the line of sight, as an indicator of the local ionization ratio. In fact, singly and doubly ionized aluminum may arise in distinct regions, in which case, $R(Al^{+2}/Al^{+})$ would reflect the relative contribution of such regions to the column densities rather than the local ionization ratio.

The $R(Al^{+2}/Al^{+})$ ratio does not show any trend with the absorber redshift. In the interval $2.0 \leq z_{abs} \leq 2.5$, where most of the measurements are concentrated, the ratio shows the full spread of a factor of 20. Since metagalactic effects are expected to have a smooth variation with redshift, the large spread in a relatively narrow redshift interval suggests that the ionization fraction is severely influenced by local effects. The metagalactic radiation field may play a role in determining the ionization balance but must be modulated by some local effect. Such modulation may result from the emission/absorption of radiation internal to the DLAs or from large changes in cloud density.

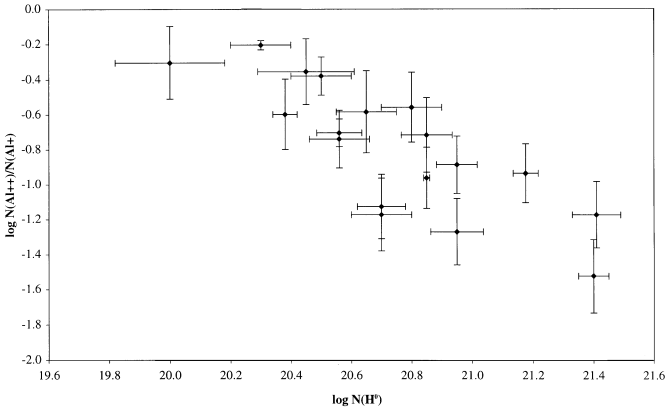

FIG. 2.—Ionization ratio $R(Al^{+2}/Al^{+})$ vs. neutral hydrogen column density in DLAs. The data points are taken from Table 1.

2.3. *Abundances versus* Al^{+2}/Al^{+} *Ionization Ratio*

The presence of high fractions of Al^{+2} with the same velocity distribution of low-ionization species might question the reliability of abundance determinations in DLAs. If abundance measurements are strongly affected by ionization conditions, we would expect that they show some dependence on $R(Al^{+2}/Al^{+})$. For instance, the models calculations performed in Paper II predict that [Zn/H] and [Si/H] measurements[2] can be easily overestimated by 1 order of magnitude when $R(Al^{+2}/Al^{+}) \geq 1/10$ for the relatively low-ionization parameters discussed in that work. The collection of $R(Al^{+2}/Al^{+})$-values presented in Table 1 allows us to probe whether such effects are indeed present, at least for elements commonly measured in DLAs. We performed a linear regression analysis of [Si/H] and [Si/Fe] against log $R(Al^{+2}/Al^{+})$. The [Si/H] analysis yields the correlation coefficient $r = 0.29$, dispersion $\sigma = 0.46$, and slope $m = 0.37 \pm 0.30$ (18 data points). The predicted increase of [Si/H] at high $R(Al^{+2}/Al^{+})$, if present, is not significant from the statistical point of view. Similar results are obtained from the study of [Si/Fe], a ratio that is expected to be moderately sensitive to ionization effects (Paper II). The [Si/Fe] analysis yields $r = 0.05$, $\sigma = 0.20$, and $m = -0.03 \pm 0.13$ (19 data points). In this case, the null result is even more clear. The lower dispersion than in the case of the Si/H ratio is probably due to the fact that variations of the metallicity and the dust-to-gas ratio tend to cancel when we consider a relative abundance such as Si/Fe. These results suggest that ionization corrections are not severe or at least that they do not show a strong, obvious dependence on $R(Al^{+2}/Al^{+})$.

2.4. Al^{+2}/Al^{+} *Ratio versus* H^0 *Column Density*

In Figure 2 we plot $R(Al^{+2}/Al^{+})$ versus the absorber H^0 column density. The data points show a general decrease of log $R(Al^{+2}/Al^{+})$ with increasing log $N(H^0)$. A linear regression analysis yields an anticorrelation with slope $m = -0.81 \pm 0.15$ and intercept $q = 16.0 \pm 3.1$. Even if

[2] We adopt the usual convention $[X/Y] = \log \{[N(X)]/[N(Y)]\} - \log (X/Y)_{\odot}$.

the correlation coefficient is not very high (Pearson's $r = -0.80$), the probability of the null hypothesis (of no correlation) is 5.9×10^{-5}. The highest value of the ratio, $R(Al^{+2}/Al^{+}) \simeq 0.6$, is found at $N(H^0) \simeq 10^{20.3}$ cm^{-2}, while the lowest value, $R(Al^{+2}/Al^{+}) \simeq 0.03$, is found at $N(H^0) \simeq 10^{21.4}$ cm^{-2}.

The above result is based in large part on indirect Al^{+} determinations obtained from Si^{+} measurements. However, the log $R(Al^{+2}/Al^{+})$–log $N(H^0)$ anticorrelation is confirmed when Fe^{+} is used to infer Al^{+} column densities. In fact, the slope and intercept derived in this case—$m = -0.78 \pm 0.16$ and $q = 15.2 \pm 3.3$—are very similar to the above given values, and the probability of the null hypothesis equals 8.6×10^{-5}.

The lack of DLAs in the bottom left- and top right-hand corners of Figure 2 could be due, in principle, to the impossibility of detecting Al^{+} and/or Al^{+2} below their observational limits. However, we have verified that this is not the case. In fact, the strength of the Al^{+} 167.0 nm transition and of the numerous Si^{+} and Fe^{+} transitions used for the indirect Al^{+} determinations guarantee that Al^{+} would be easily detected down to much lower column densities than observed. In the case of Al^{+2}, the detection limit with Keck HIRES is $\simeq 10^{12}$ cm^{-2}. In the sample of Table 1, only one case out of 21 measurements has such a low value. Of the remaining $N(Al^{+2})$ data, nine are 0.5 dex above the detection limit and 11 are 1 dex above the limit. We conclude that the anticorrelation is not an artifact induced by observational limitations.

In addition, we do not have reasons to believe that the observed trend results from a selection bias. The most common bias considered to affect the population of DLAs is dust obscuration of the background QSO (Pei, Fall, & Bechtold 1991). In fact, this effect may be responsible for the apparent anticorrelation between [Zn/H] and $N(H^0)$ found by Boissé et al. (1998) if the lines of sight of high metallicity (dust content) and high column density indeed obscure the background QSO. However, the same effect should not be relevant for the anticorrelation reported here given the fact that the ratio $R(Al^{+2}/Al^{+})$ is independent of metallicity.

The existence of an empirical anticorrelation log $N(H^0)$–log $R(Al^{+2}/Al^{+})$ implies that the neutral hydrogen column density can be used as an indirect estimator of the ionization state of the gas. In this way, one can search for ionization effects in DLAs without available Al measurements. Given the importance of Zn in DLA studies, we searched for a possible dependence of [Cr/Zn] and [Fe/Zn] on log $N(H^0)$. A linear regression through the 26 [Cr/Zn] measurements available yields a slope of $m = -0.03 \pm 0.11$ and a correlation coefficient $r = 0.06$. Very similar results are obtained from the analysis of the 22 [Fe/Zn] available determinations: $m = -0.04 \pm 0.13$ and $r = 0.07$. In addition, there is no trace of an increased dispersion at low $N(H^0)$ for any of the two ratios. These empirical results suggest that Zn ionization effects are probably negligible in DLAs.

If Al^{+2}/Al^{+} is relatively constant throughout the cloud, the $R(Al^{+2}/Al^{+})$ ratio should be approximately constant with $N(H^0)$. The decrease of $R(Al^{+2}/Al^{+})$ with $N(H^0)$ can be interpreted in two ways depending on which of the two possible origins of Al^{+2} mentioned at the end of § 2.1 is more appropriate. (1) If Al^{+2} is cospatial with the rest of low-ionization species, the anticorrelation is consistent with a reduction of the gas ionization level with increasing H^0 self-shielding. (2) If Al^{+2} originates in a partially ionized interface bordering a neutral region, then we expect the column density of the ionized interface and of the neutral region to be unrelated and, therefore, $N(Al^{+2})$ to be independent of $N(H^0)$. On the other hand, we expect Al^{+} and other species of low ionization to scale with H^0 owing to a common origin in the neutral region. The decrease of $R(Al^{+2}/Al^{+})$ with $N(H^0)$ is naturally explained from the fact that $N(Al^{+2})$ does not scale with $N(H^0)$ while $N(Al^{+})$ does.

3. MODEL CALCULATIONS

On the basis of the observational results discussed above, we consider two possible origins for species of low and intermediate ionization: (1) regions completely opaque to photons with $h\nu > 13.6$ eV and/or (2) regions partially transparent to ionizing photons. Neutral and singly ionized species can arise in both regions, but Al^{+2} can only be present in type 2 regions. The general idea is that type 2 regions are the photoionized envelopes of type 1 regions. The similarity of the velocity profiles of Al^{+2} and singly ionized species is naturally explained in this way. On the other hand, radial velocity studies show a general misalignment of C^{+3} and Si^{+3} profiles relative to Al^{+2} profiles, suggesting that the bulk of high-ionization species originates elsewhere (Wolfe & Prochaska 2000). We therefore expect that type 2 regions are mildly ionized and have a low Si^{+3}/Si^{+} fraction.

In Appendix A we derive the expressions that allow us to compute ionization ratios and abundance ionization corrections in the framework of the two-region model. These expressions do not depend on the metallicity, provided that type 1 and type 2 regions have equal metallicity in any given DLA system. The relative contribution of the two regions along the line of sight is specified by the parameter N_1/N_2, which is the ratio of the total column densities in region 1 and 2, respectively. The possibility that Al^{+2} and the species of low ionization originate together in a single layer is included in our treatment as the special case $N_1/N_2 = 0$. In fact, the single layer should be a partially ionized region of type 2 given the presence of significant fractions of Al^{+2}.

In order to model the ionization properties of the gas, we assume that the DLA regions under study are embedded in a ionizing radiation field of a given spectrum and intensity. In type 1 regions we only consider the contribution of species that are dominant ionization states in H I regions. In type 2 regions we compute the ionization fractions by means of photoionization equilibrium calculations. For this purpose, we used the CLOUDY code (v90.04; Ferland 1996; Ferland et al. 1998) assuming plane-parallel geometry with ionizing radiation incident on one side. We consider two possible types of radiation fields: a hard, QSO-dominated spectrum representative of the radiation field external to the DLAs at $z = 2$ (Haardt & Madau 1996; Madau, Haardt, & Rees 1999) and a soft, stellar-type spectrum ($T_{\rm eff} = 33{,}000$ K; Kurucz 1991) representative of the internal radiation field or of an external field dominated by starlight from galaxies (see, e.g., Steidel, Pettini, & Adelberger 2001). In both cases, the intensity of the field is specified by the ionization parameter $U \equiv \Phi(H)/cn_H$, where $\Phi(H)$ is the total surface flux of ionizing photons (in units of cm^{-2} s^{-1}) and n_H is the hydrogen particle density (in units of cm^{-3}). We refer to Paper II for more details on the model assumptions and on the adopted radiation fields. In the rest of this section we present model predictions of the ioniza-

tion ratios $R(Al^{+2}/Al^{+})$ and of the abundance ionization corrections.

3.1. *Aluminum Ionization Ratio*

3.1.1. *Soft-Continuum, Two-Region Model (S2 Model)*

The photoionization calculations indicate that with the soft, stellar-type spectrum, the H^0 column density of the ionized layer $N_2(H^0)$ cannot attain the high values typical of DLAs for a wide range of U. In fact, we find $N_2(H^0) \leq 3.2 \times 10^{18}$ cm^{-2} for $-5.4 \leq \log U \leq -1.0$. Therefore, we assume that a neutral region of type 1 is present along the line of sight in addition to the Al^{+2}-bearing, type 2 region. We refer to this soft-continuum, two-region model as S2.

Because the ionized region does not yield a significant contribution to the neutral hydrogen column density and because $x(H^0) = 1$ in the neutral region, we take $N_1(H) = N_1(H^0) = N(H^0)$ as the total column density of the type 1 region, where $N(H^0)$ covers the interval $10^{20.2}$ cm$^{-2} < N(H^0) < 10^{22}$ cm^{-2}, which is representative of DLAs. For each given $N_1(H)$, we let the ionization parameter U vary, and we use CLOUDY to determine the column density of the type 2 region, $N_2(H)$, and the mean ionization fractions of the species of interest. We then estimate $R(Al^{+2}/Al^{+})$ by means of equation (A7), where we take $N_1/N_2 = N_1(H)/N_2(H)$ and we insert the Al^{+} and Al^{+2} ionization fractions. In this way, we derive model curves of $R(Al^{+2}/Al^{+})$ versus $N(H^0)$ that can be compared with the observed data points.

In Figure 3 we show the results of these calculations for constant values of the ionization parameter. The solutions calculated at $U = 10^{-2.2}$ (*thick curve*) are consistent, within the statistical errors, with the linear regression of the observational data points (*dash-dotted line*). The corresponding total hydrogen column density of the type 2 layer predicted by the model is $N_2(H) = 8 \times 10^{20}$ cm^{-2}. The solutions calculated at $U_{min} = 10^{-2.6}$ and $U_{max} = 10^{-1.7}$ (*lower and upper thin curves, respectively*) bracket the observational data points. For these lower and upper envelope curves, we find $N_2(H) = 3.3 \times 10^{20}$ and 2.3×10^{21} cm^{-2}, respectively. The total column densities of type 1 and type 2 regions are roughly comparable ($N_1/N_2 \approx 1$). It is remarkable that the log $N(H^0)$–log $R(Al^{+2}/Al^{+})$ anticorrelation can be easily modeled with very simple assumptions and with a single interval of U-values in the framework of the S2 model.

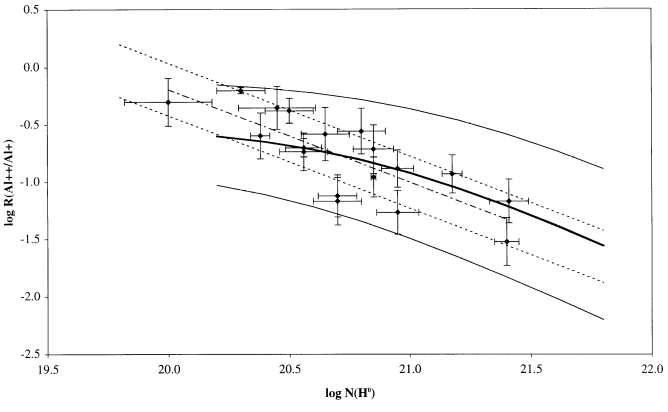

FIG. 3.—Model predictions of the $R(Al^{+2}/Al^{+})$ ratio vs. $N(H^0)$ in DLAs in the case of a soft, stellar ionizing source (model S2 discussed in § 3.1.1). *Solid curves*: log $R(Al^{+2}/Al^{+})$ predicted at log $U = -2.6$ (*bottom curve*), -2.2 (*thick line*), and -1.7 (*top curve*). *Diamonds*: Observational data points as in Fig. 2; *dash-dotted line*: linear regression through the observed data; *dotted lines*: $\pm 1\ \sigma$ dispersion of the linear regression.

3.1.2. *Hard-Continuum, Single-Region Model (H1 Model)*

With the QSO-dominated field, the H^0 column density of the ionized layer can attain the high values typical of DLAs if U is sufficiently high. As a consequence, the presence of a of type 1 region is not required in order to explain the observed $N(H^0)$-values. In this case, we assume that all the low- and intermediate-ionization species originate in a single, partially ionized layer. We refer to this hard-continuum, one-region model as H1. We stopped the calculations at a series of $N(H^0)$-values representative of DLAs rather than at a given threshold of the ionization fraction. Our treatment of this case is therefore quite similar to those of Lu et al. (1995) and Prochaska & Wolfe (1996). At variance with the S2 model, in the H1 model there is residual ionized gas, and hence Al^{+2}, throughout the interior of the cloud due to the strong high-energy tail of the extragalactic Haardt & Madau spectrum. In Figure 4 we show the resulting $R(Al^{+2}/Al^{+})$ ratios plotted versus $N(H^0)$ at constant values of U. We estimated $R(Al^{+2}/Al^{+})$ from equation (A7) by taking $N_1/N_2 = 0$. When U is too low, there are difficulties with the thermal solution in the CLOUDY computation since the temperature falls well below 1000 K before the total $N(H^0)$ is reached. This explains the lack of solutions below log $U = -4.8$ in Figure 4. On the other hand, some of the solutions tend to overproduce Si^{+3} when U is too high. As an example, in Figure 4 we indicate with open circles the solutions for which $R(Si^{3+}/Si^{+}) > -0.5$ dex. The intrinsic $R(Si^{3+}/Si^{+})$ is probably much lower than this conservative limit given the very different velocity structure of Si^{3+} and Si^{+}.

With the H1 model, the curves predicted at constant U have very different—in some cases opposite—slopes from that of the anticorrelation log $N(H^0)$–log $R(Al^{+2}/Al^{+})$ (Fig. 4). When all the U-values are considered, the solutions tend to fill the plane log $N(H^0)$–log $R(Al^{+2}/Al^{+})$ without any preference for the regions populated by observational data. To reproduce the anticorrelation, it is necessary to impose

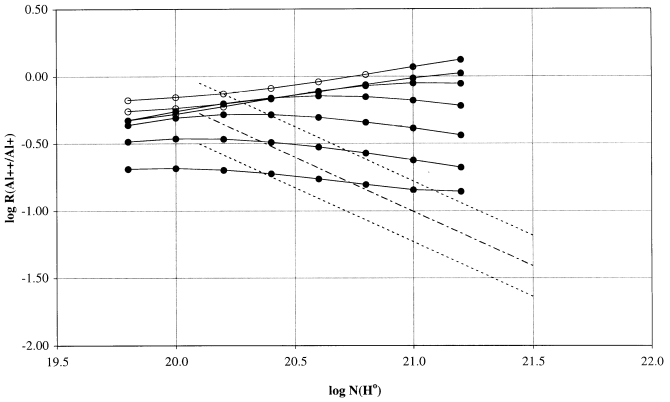

FIG. 4.—Model predictions of the $R(Al^{+2}/Al^{+})$ ratio vs. $N(H^0)$ in DLAs in the case of a hard, QSO-dominated ionizing source (model H1 discussed in § 3.1.2). The continuous curves have been obtained at constant value of the photoionization parameter U. The curves from bottom to top correspond to log $U = -4.8$, -4.2, -3.6, -3.0, -2.4, -1.8, and -1.2, respectively. The filled and open symbols represent solutions for which $R(Si^{+3}/Si^{+}) \leq -0.5$ dex and $R(Si^{+3}/Si^{+}) > -0.5$ dex, respectively. The dash-dotted line represents the linear regression through the observed data points. The dotted lines represent the $\pm 1\ \sigma$ dispersion of the linear regression trough the observed data.

very specific constraints on the input parameters. For a given $N(H^0)$, there is an allowed interval of U-values such that the predicted $\log R(Al^{+2}/Al^{+})$ ratios overlap the observed ones. For instance, at $\log N(H^0) = 20.4$, we must require that $-4.8 \lesssim \log U \lesssim -3.6$ in order to obtain ratios that lie within $\pm 1\ \sigma$ of the regression to the observed data points (Fig. 4). In addition, the ionization parameter must decrease, on the average, while $N(H^0)$ increases. For instance, we must require that $U \propto N(H^0)^{-1.5}$ in order to reproduce the slope of the observed anticorrelation in the range $20.4 \leq \log N(H^0) \leq 20.8$. This is at variance with the results of the S2 model, for which all the observed data points are easily matched by adopting a single interval of U-values.

The use of one-sided illuminated clouds is inherent to the design of CLOUDY, but may be slightly inappropriate for the external, hard ionizing spectrum case. According to Prochaska & Wolfe (1996), one-sided calculations tend to give a lower degree of ionization than two-sided calculations. We have estimated this effect by doubling the column densities of the one-sided calculations. With this type of estimate, we do not find significant changes in the results of the present work, including the abundance corrections discussed below.

3.2. *Abundance Ionization Corrections*

Abundance determinations in DLAs are based on column density measurements of species that are dominant ionization states in H^0 regions. In Appendix A we define the ionization correction terms that allow us to recover the intrinsic abundances starting from this type of measurement. In order to estimate these correction terms, we used the same sets of input parameters—ionizing spectrum, U, and N_1/N_2—that allow us to reproduce the observed $[N(H^0), R(Al^{+2}/Al^{+})]$ distribution. In practice, with such parameters, we determine the mean ionization fractions $\overline{x}_2(X^i)$ with CLOUDY and the correction terms from equations (A5) and (A6). Thanks to this procedure, the input parameters are constrained by the requirement to model the Al^{+2}/Al^{+} observations. An additional advantage is that the ionization effects are estimated as a function of $N(H^0)$, which is a measurable quantity. In this way, the range of predicted ionization corrections is reduced once we know $N(H^0)$ for individual DLAs. The resulting corrections for absolute abundances are shown in Figures 5–16. In each figure we display the corrections predicted by the S2 and H1 models discussed above. Corrections for N/H and O/H are not shown in the figures because they are always below the abundance measurement errors ($\lesssim 0.05$ dex).

The corrections estimated with the S2 model are shown in Figures 5–16 (absolute abundances) and Table 3 (relative abundances). In the S2 model the species used for abundance measurements arise mostly in type 1 neutral regions, with an additional contribution from type 2 ionized regions. It is this latter contribution that affects the measured abundances. The correction terms predicted by this model are generally small owing to the high U-values that we require to match the $R(Al^{+2}/Al^{+})$ versus $N(H^0)$ data. In fact, when U is high, the species used for abundance measurements tend to vanish in the ionized region since they move to a higher state of ionization. Ionization corrections tend to decrease in absolute value with increasing $N(H^0)$. This is due to the fact that the relative contribution of the ionized layer becomes less important at high $N(H^0)$.

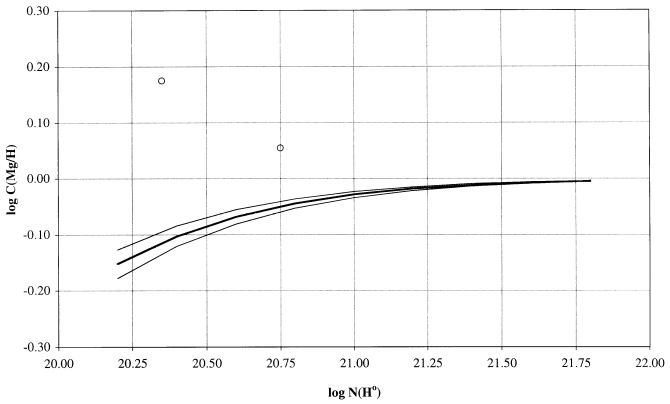

FIG. 5.—Ionization correction terms for [Mg/H] measurements in DLAs. *Solid curves*: Predictions for the S2 model discussed in § 3.1.1 calculated at constant values of the ionization parameter U. *Thick curve*: $\log U = -2.2$. *Thin curves*: $\log U = -1.7$ (*bottom*) and $\log U = -2.2$ (*top*). *Open circles*: Predictions for the H1 model discussed in § 3.1.2 calculated at $\log U = -4.2$ (*left*) and $\log U = -4.8$ (*right*).

The predictions for the H1 model have been derived by considering only the solutions that match the empirical $\log N(H^0)$–$\log R(Al^{+2}/Al^{+})$ anticorrelation. The open circles in Figures 5–16 have been calculated using the solutions found at the intersection between the linear regression to the data points and the curves at the constant ionization parameter $\log U = -4.2$ and -4.8 shown in Figure 4. Owing to the difficulty of finding solutions at lower U and high $N(H^0)$, we have not calculated corrections at $\log N(H^0) \geq 21$. It is clear, however, that the correction terms become negligible at high $\log N(H^0)$. The reason for this is that the corrections decrease (in absolute value) with decreasing U and, at the same time, $U \propto N(H^0)^{-1.5}$. The predicted corrections are generally small because the match with the observed $R(Al^{+2}/Al^{+})$ ratios is found at low values of U.

The correction terms can be negative or positive depending on the model adopted and on the species considered. The corrections for absolute abundances X/H are negative in the S2 model. In this model the dominant species used for the measurements, X^{id} and H^0, mostly arises in the type 1 region unaffected by ionization; the type 2 layer gives an extra contribution that enhances the X^{id}/H^0 ratio, and a negative correction is required to recover the intrinsic abundance. In the H1 model the corrections for absolute abundances can be negative or positive since all the species arise in a single layer in which the X^{id}/H^0 ratio can be larger or smaller than the intrinsic abundance.

3.3. *Accuracy of* Al *Atomic Data*

The above calculations rely on the accuracy of the input atomic data. Here we are particularly interested in the accuracy of the Al data since our models are constrained by the capability of matching the observed $\log N(H^0)$–$\log R(Al^{+2}/Al^{+})$ anticorrelation. The photoionization cross sections currently used in CLOUDY calculations are generally accurate within $\simeq 10\%$, the Al^{+} cross section having a regular level of accuracy (Verner et al. 1996; Ferland et al. 1998). Radiative recombination rate coefficients can be obtained with an accuracy better than $\simeq 15\%$ (Ferland et al. 1998). However, the recombination process can be dominated by dielectronic recombination (DR), which is a far more uncertain mechanism. Low-temperature DR rates,

TABLE 3

IONIZATION CORRECTION TERMS FOR ABUNDANCE RATIOS IN DLA SYSTEMS[a]

	log $N(H^0)$								
CORRECTION TERM	20.2	20.4	20.6	20.8	21.0	21.2	21.4	21.6	21.8
C[N/O]	+0.002	+0.001	+0.001	+0.001	+0.000	+0.000	+0.000	+0.000	+0.000
C[N/Si]	+0.149	+0.100	+0.066	+0.043	+0.028	+0.018	+0.011	+0.007	+0.004
C[N/S]	+0.227	+0.157	+0.105	+0.070	+0.045	+0.029	+0.019	+0.012	+0.007
C[N/Fe]	+0.027	+0.017	+0.011	+0.007	+0.004	+0.003	+0.002	+0.001	+0.001
C[N/Zn][b]	+0.642	+0.498	+0.372	+0.269	+0.188	+0.128	+0.085	+0.055	+0.036
C[O/Mg]	+0.152	+0.102	+0.068	+0.044	+0.028	+0.018	+0.011	+0.007	+0.005
C[O/Si]	+0.147	+0.099	+0.065	+0.042	+0.027	+0.017	+0.011	+0.007	+0.004
C[O/S]	+0.225	+0.155	+0.105	+0.069	+0.045	+0.029	+0.018	+0.012	+0.007
C[O/Fe]	+0.025	+0.016	+0.010	+0.006	+0.004	+0.003	+0.002	+0.001	+0.001
C[O/Zn][b]	+0.640	+0.496	+0.371	+0.268	+0.187	+0.127	+0.085	+0.055	+0.036
C[Mg/Si]	−0.005	−0.004	−0.002	−0.002	−0.001	−0.001	−0.000	−0.000	−0.000
C[Mg/S]	+0.073	+0.053	+0.037	+0.025	+0.017	+0.011	+0.007	+0.004	+0.003
C[Mg/Fe]	−0.127	−0.086	−0.057	−0.037	−0.024	−0.015	−0.010	−0.006	−0.004
C[Mg/Zn][b]	+0.488	+0.394	+0.304	+0.224	+0.159	+0.109	+0.073	+0.048	+0.031
C[Al/Si]	−0.531	−0.431	−0.334	−0.249	−0.178	−0.123	−0.082	−0.054	−0.035
C[Al/Fe]	−0.653	−0.514	−0.389	−0.284	−0.201	−0.137	−0.092	−0.060	−0.039
C[Al/Zn][b]	−0.038	−0.033	−0.028	−0.023	−0.017	−0.013	−0.009	−0.006	−0.004
C[Si/Fe]	−0.122	−0.083	−0.055	−0.036	−0.023	−0.015	−0.009	−0.006	−0.004
C[Si/Zn][b]	+0.493	+0.397	+0.306	+0.226	+0.160	+0.110	+0.074	+0.048	+0.031
C[P/Si]	−0.150	−0.111	−0.079	−0.054	−0.036	−0.024	−0.015	−0.010	−0.006
C[P/Fe]	−0.272	−0.194	−0.134	−0.090	−0.059	−0.039	−0.025	−0.016	−0.010
C[P/Zn][b]	+0.343	+0.286	+0.227	+0.172	+0.124	+0.086	+0.058	+0.038	+0.025
C[S/Si]	−0.078	−0.057	−0.039	−0.027	−0.018	−0.011	−0.007	−0.005	−0.003
C[S/Fe]	−0.200	−0.139	−0.094	−0.063	−0.041	−0.026	−0.017	−0.011	−0.007
C[S/Zn][b]	+0.415	+0.341	+0.267	+0.199	+0.143	+0.098	+0.066	+0.044	+0.028
C[Ti/Si]	+0.083	+0.057	+0.038	+0.025	+0.016	+0.010	+0.007	+0.004	+0.003
C[Ti/Fe]	−0.039	−0.026	−0.017	−0.011	−0.007	−0.004	−0.003	−0.002	−0.001
C[Ti/Zn][b]	+0.576	+0.454	+0.344	+0.251	+0.176	+0.120	+0.08	+0.052	+0.034
C[Cr/Si]	+0.134	+0.091	+0.060	+0.039	+0.025	+0.016	+0.010	+0.006	+0.004
C[Cr/Fe]	+0.012	+0.008	+0.005	+0.003	+0.002	+0.001	+0.001	+0.001	+0.000
C[Cr/Zn][b]	+0.627	+0.488	+0.366	+0.265	+0.185	+0.126	+0.084	+0.055	+0.035
C[Mn/Si]	+0.086	+0.059	+0.039	+0.026	+0.017	+0.011	+0.007	+0.004	+0.003
C[Mn/Fe]	−0.036	−0.024	−0.016	−0.01	−0.006	−0.004	−0.003	−0.002	−0.001
C[Mn/Zn][b]	+0.579	+0.456	+0.346	+0.252	+0.177	+0.121	+0.080	+0.053	+0.034
C[Ni/Si]	+0.042	+0.029	+0.020	+0.013	+0.009	+0.005	+0.004	+0.002	+0.001
C[Ni/Fe]	−0.080	−0.054	−0.035	−0.023	−0.015	−0.009	−0.006	−0.004	−0.002
C[Ni/Zn][b]	+0.535	+0.427	+0.326	+0.239	+0.169	+0.115	+0.077	+0.050	+0.033
C[Zn/Fe]	−0.615	−0.480	−0.361	−0.262	−0.183	−0.125	−0.083	−0.054	−0.035

[a] Results predicted by model S2 at log $U = -2.2$ (see § 3.1). All values are given in logarithm.
[b] Systematic errors probably are present owing to uncertainty of zinc atomic parameters.

which are critical for determining the ionization balance in the photoionization equilibrium, are lacking for many elements (Ferland et al. 1998). Luckily, such coefficients have been calculated for Al. However, given the theoretical and experimental uncertainties, it is possible that the Al^+ DR rate may be overestimated (Nussbaumer & Storey 1986). If the Al^+ recombination rate is overestimated, the predicted $R(Al^{+2}/Al^+)$ ratio is underestimated. An effect of this type has been reported in a photoionization study of a Lyman limit system, in which the models that give a good fit to other species are not able to reproduce the relatively high $R(Al^{+2}/Al^+)$ ratio observed (D'Odorico & Petitjean 2001). In order to test the consequences of an effect of this type, we artificially increased the ratio $R(Al^{+2}/Al^+)$ calculated at any given value of U. The results that we found can be summarized as follows. In the S2 model (1) the observed anticorrelation is matched at lower U-values; (2) the column density N_2 of the ionized layer, which scales with U, becomes lower; (3) the ionization corrections, which scale with N_2, become lower; and (4) the Al correction becomes even lower (in absolute value) owing to the reduced contribution of Al^+ from the ionized layer. In the H1 model (1) the solutions that match the observed anticorrelation are shifted to lower U-values and (2) the ionization corrections, which in this case scale with U, become lower. In summary, if the Al recombination rate is too high, then the ionization parameter U and the abundance corrections calculated above should be reduced; in particular, the Al abundance corrections of model S2 would be more in line with those of the other elements.

3.4. *Implications for the Indirect Estimates of* $N(Al^+)$

The large values of Al correction terms that we find are somewhat surprising given the fact that most Al^+ column densities have been indirectly estimated from Si^+ column densities.[3] In fact, the log $N(Al^+)$–log $N(Si^+)$ correlation could, in principle, be destroyed by the large ionization

[3] This discussion could be equally applied to the indirect estimates based on Fe^+ column densities.

effects predicted. Since this is not the case, we must understand why. One possible reason is that, owing to the uncertainty of the Al^+ recombination coefficients, the Al correction terms may be overestimated, as we have discussed above. Another possibility is that the Al correction terms are correct, but the correlation is not destroyed because we are considering a limited interval of $N(H^0)$. In fact, in the column density range of the DLAs used for deriving the $\log N(Al^+)$–$\log N(Si^+)$ correlation—i.e., $20.3 < \log N(H^0) < 20.7$—the Al/Si corrections terms are large, but nevertheless, they only show a modest variation ($\approx \pm 0.1$ dex). As a consequence, the ionization effects may significantly change the intercept of the $\log N(Al^+)$–$\log N(Si^+)$ correlation but should not change significantly the dispersion and the slope.

The $N(Al^+)$-values inferred from $N(Si^+)$ may contain a systematic error when $\log N(H^0) > 20.7$ owing to the variation of $C(Al/Si)$ with $N(H^0)$. If the Al correction terms are overestimated, the effect is probably small. Otherwise, we can quantify this error from the predicted variation of $\log C(Al/Si)$ between $\log N(H^0) \simeq 20.5$ and $\log N(H^0) \simeq 21.5$. We find that $N(Al^+)$ may be overestimated by $\simeq 0.2/0.3$ dex in model S2 or underestimated by a similar amount in model H1. These values are generally within the error bars quoted in the last column of Table 1. In any case, these errors would not affect the results of the present work. In the case of model S2, in order to compensate for such errors, we should decrease $N(Al^+)$ and hence increase $R(Al^{+2}/Al^+)$ by $\simeq 0.2/0.3$ dex at $\log N(H^0) > 20.7$. One can see from Figure 3 that such an increase would even improve the agreement between the S2 model and the observations. In the case of the H1 model, we should instead decrease $R(Al^{+2}/Al^+)$. This would imply that the interval (U_{min}, U_{max}) of allowed solutions should be slightly shifted to lower U-values at high $\log N(H^0)$.

4. IMPLICATIONS FOR ABUNDANCE STUDIES

We briefly discuss how the ionization correction terms presented here can affect studies of DLA abundances. Unless differently specified, the results summarized below are relative to both types of models considered in this work.

The correction terms for N and O are generally negligible. This is not surprising since the ionization fractions of H^0, N^0, and O^0 are held together because of the strong charge exchange reactions (see, e.g., Sembach et al. 2000). We note, however, that cosmic-ray ionization can affect the N^0/O^0 ratio (Viegas 1995). The [N/Si] ratio is slightly underestimated (Table 3). The correction term for [N/S] can be positive or negative, depending on the adopted model. In any case, the effect is generally small, with $|\log C(N/S)| \lesssim +0.2$ dex for $N(H^0) \geq 20.3$. These results indicate that the large scatter of [N/Si] and [N/S] abundances found by Lu, Sargent & Barlow (1998) and by Centurión et al. (1998) is a genuine nucleosynthetic effect. Claims that nitrogen abundances are severely affected by ionization effects (Izotov & Thuan 1999) are not supported by our study.

The correction terms for Al may be quite large but with different signs depending on the model adopted (Fig. 6). Measurements of the Al/Fe and Al/Si ratios in DLAs yield $[Al/Fe] \approx 0$, with a scatter of $\simeq 0.3$ dex, and $[Al/Si] \approx -0.4$ dex, with values between -0.1 and -0.6 dex (Prochaska & Wolfe 1999). Local interstellar medium studies indicate that Al and Fe have similar depletion

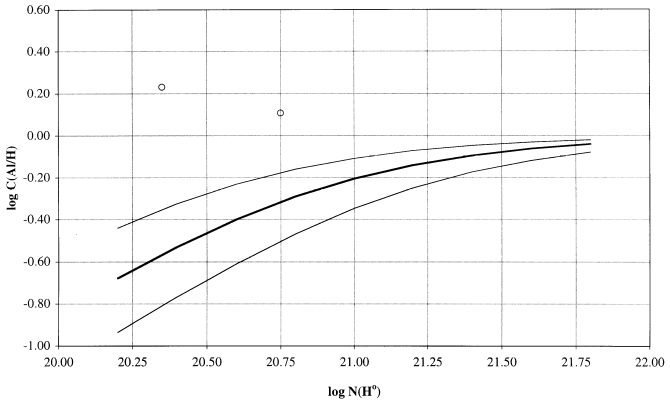

FIG. 6.—Ionization correction terms for [Al/H] measurements. The symbols are the same as in Fig. 5.

(Barker et al. 1984; Howk, Savage, & Fabian 1999). The [Al/Fe] ratios should not be affected by depletion, while the [Al/Si] ones should be affected as much as the [Fe/Si] ratios, which are underestimated by ≈ 0.3 dex in DLAs (Paper I). So we expect $[Al/Fe] \approx 0$ and $[Al/Si] \approx -0.1$ dex after correcting for dust. For the DLAs with available Al^+ measurements, we predict $\log C(Al/Fe) \approx \log C(Al/Si) \approx -0.4$ (S2 model) or $\approx +0.2$ dex (H1 model). Therefore, after dust and ionization corrections are applied, the [Al/Fe] and [Al/Si] ratios are below solar in the S2 model but somewhat enhanced in the H1 model. As we mentioned above, these ionization effects may be weaker if the Al^+ recombination rate is overestimated.

Silicon and sulphur are used as a tracers of α-elements given the difficulty of measuring oxygen in DLAs. The [Si/H] correction term is $\simeq -0.1$ dex at $\log N(H^0) \simeq 20.3$ (Fig. 7), and silicon abundances can be accordingly overestimated. However, the effect is not strong, and this may explain why [Si/H] measurements in DLAs do not show a trend with $R(Al^{+2}/Al^+)$, as discussed in § 2.3. The [S/H] corrections terms are negative for the S2 model and positive for the H1 model, in both cases being $\lesssim 0.2$ dex in absolute value (Fig. 9).

The [Si/Fe] ratio, which is used as a proxy of the α/Fe ratio, shows an enhancement of $\simeq 0.3/0.5$ dex in DLAs, which has been interpreted as an intrinsic nucleosynthetic effect (see, e.g., Lu et al. 1996) or as a differential dust depletion (see, e.g., Paper I). The present study indicates that [Si/Fe] is almost unaffected by ionization corrections, being

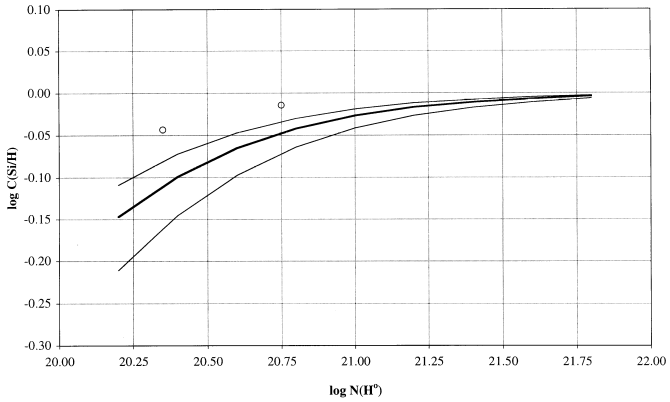

FIG. 7.—Ionization correction terms for [Si/H] measurements. The symbols are the same as in Fig. 5.

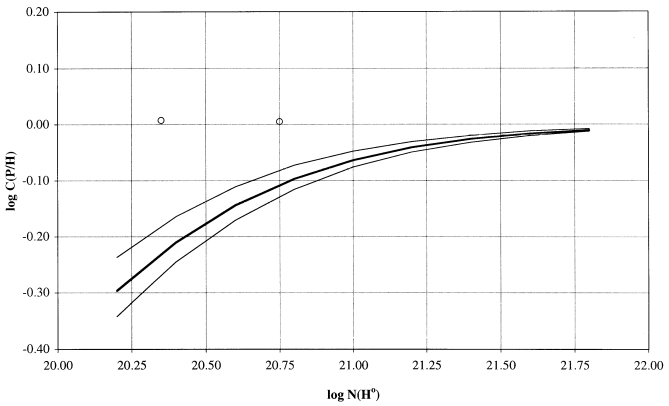

FIG. 8.—Ionization correction terms for [P/H] measurements. The symbols are the same as in Fig. 5.

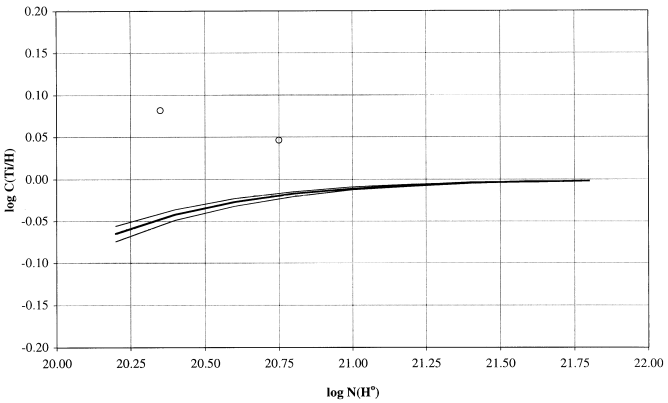

FIG. 11.—Ionization correction terms for [Ti/H] measurements. The symbols are the same as in Fig. 5.

possibly overestimated by $\simeq 0.1$ dex at low $N(H^0)$ in the S2 model. Owing to the negligible dust depletion of both sulphur and zinc, the [S/Zn] ratio has been used as a dust-free [α/Fe] indicator in DLAs (Centurión et al. 2000; see, however, Prochaska et al. 2000). The correction terms for the [S/Zn] ratio are ≈ 0.2 dex in absolute value for the DLAs with available S measurements. Considering that such corrections are dominated by the zinc contribution that may be overestimated (see below), we conclude that the [S/Zn] results presented by Centurión et al. (2000) are modestly affected by ionization effects. Local interstellar studies yield an S/Zn ratio that is approximately solar (Howk, Savage, & Fabian 1999), suggesting that ionization corrections are unimportant.

Ionization effects tend to lower the measured Ar abundances in the local interstellar medium, at least in lines of sight with log $N(H^0) \leq 20.0$ (Sofia & Jenkins 1998; Jenkins et al. 2000). In DLAs the Ar corrections are negligible in the case of the S2 model; however, Ar may be severely underestimated in the H1 model when the H^0 column density is low (Fig. 10).

Corrections for Cr and Fe are $\lesssim 0.05$ dex in absolute value (Figs. 12 and 14), and those for Ti, Mn, and Ni are

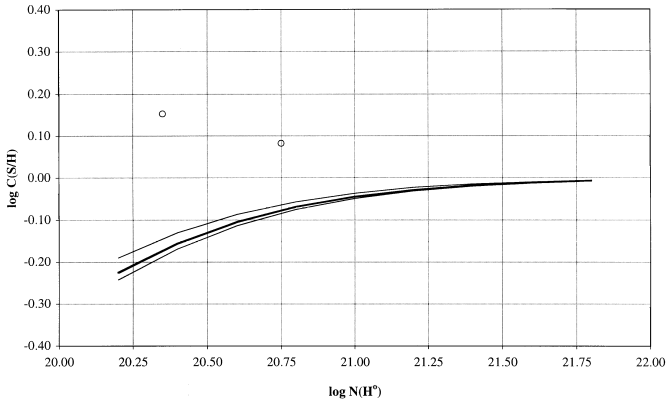

FIG. 9.—Ionization correction terms for [S/H] measurements. The symbols are the same as in Fig. 5.

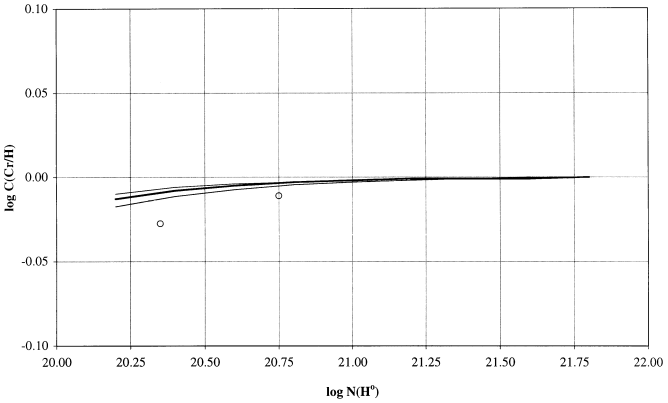

FIG. 12.—Ionization correction terms for [Cr/H] measurements. The symbols are the same as in Fig. 5.

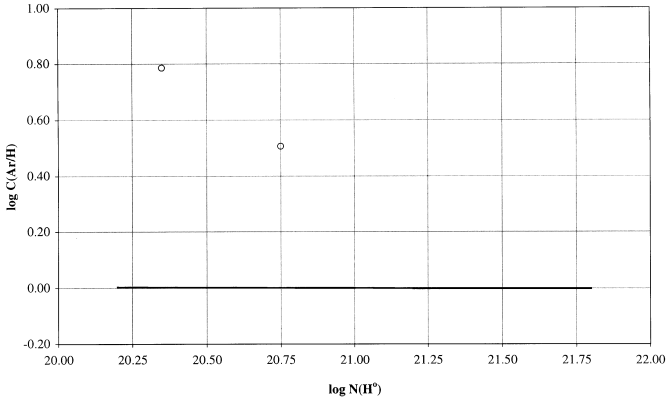

FIG. 10.—Ionization correction terms for [Ar/H] measurements. The symbols are the same as in Fig. 5.

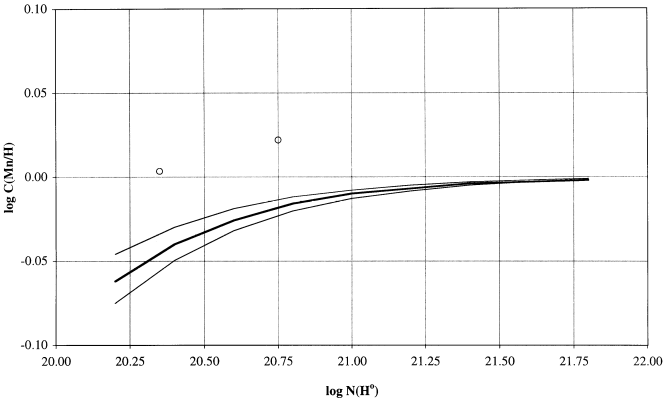

FIG. 13.—Ionization correction terms for [Mn/H] measurements. The symbols are the same as in Fig. 5.

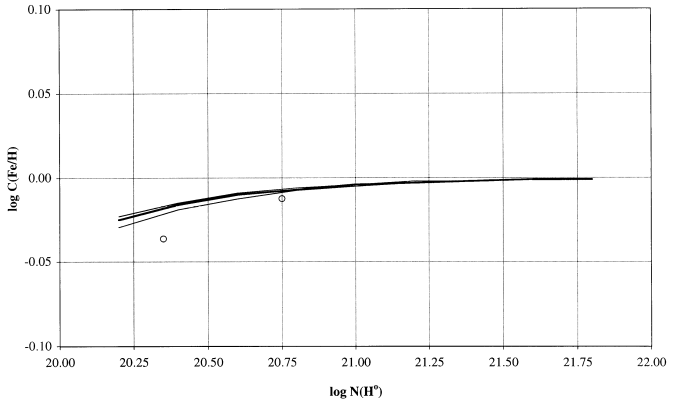

FIG. 14.—Ionization correction terms for [Fe/H] measurements. The symbols are the same as in Fig. 5.

$\lesssim 0.1$ dex (Fig. 11, 13, and 15, respectively). Therefore, deviations from solar ratios observed for pairs of iron peak elements such as [Cr/Fe] and [Mn/Fe] (Lu et al. 1996; Prochaska & Wolfe 1999) must be due either to dust depletion or to nucleosynthetic effects since ionization effects are excluded.

The predicted corrections for Zn are relatively large, with opposite signs depending on the model adopted (Fig. 16). Owing to the predicted variation of the Zn correction terms with log $N(H^0)$, we would expect to find some trend between the [Cr/Zn] and [Fe/Zn] ratios and log $N(H^0)$. The lack of any trend (see § 2.4) suggests that the zinc correction terms may be overestimated. This could be the case

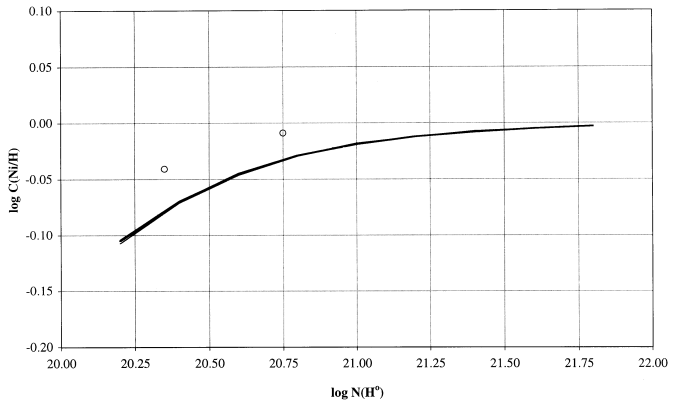

FIG. 15.—Ionization correction terms for [Ni/H] measurements. The symbols are the same as in Fig. 5.

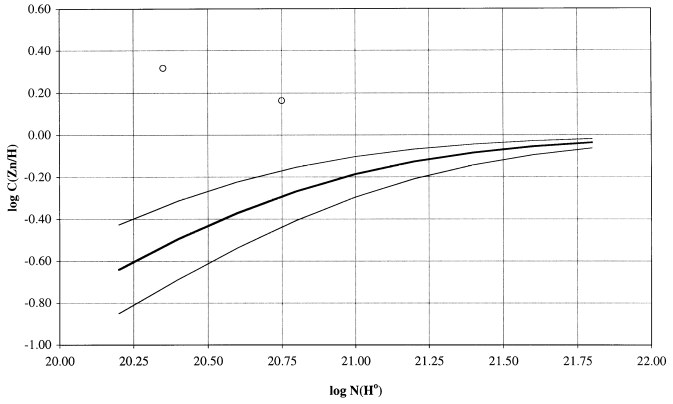

FIG. 16.—Ionization correction terms for [Zn/H] measurements. The symbols are the same as in Fig. 5.

since the Zn recombination coefficients and ionization cross sections are rather uncertain (Howk, Savage, & Fabian 1999).

5. SUMMARY AND CONCLUSIONS

We have analyzed column density measurements of Al^{+2} and of singly ionized species available in the literature to cast light on the properties of low-ionization regions in DLA systems. We have found that log $N(Al^+)$ is well correlated with log $N(Si^+)$ and log $N(Fe^+)$, and we have used this result to estimate $N(Al^+)$ and the ratio $R(Al^{+2}/Al^+) = N(Al^{+2})/N(Al^+)$ for a sample of 20 DLAs. The ratio can attain relatively high values, up to $\simeq 0.6$, with a median value of 0.2. This result is contrary to the common belief that the fraction of Al^{+2} is generally small in DLAs. In the redshift interval $2.0 \leq z_{abs} \leq 2.5$, where most of the measurements are concentrated, the ratio shows the full spread of a factor of 20. Therefore, the ratio must be influenced by local effects not dependent on z_{abs}. Local absorption and/or local radiation fields probably play an important role in determining the ionization properties inside DLAs.

The presence of high fractions of Al^{+2} with the same velocity distribution of low ionization may question the reliability of abundance determinations in DLAs. We have investigated the behavior of [Si/H] and [Si/Fe] abundance ratios in order to put in evidence possible effects of ionization. However, we do not find any trend between these abundance ratios and $R(Al^{+2}/Al^+)$. We have considered the possibility that Al^{+2} originates in a region different from the one where species of low ionization arise. In this case, the ratio $R(Al^{+2}/Al^+)$ would measure the relative contribution of different regions rather than the intrinsic degree of ionization of a single region. From a regression analysis of the logarithmic column densities, we find some evidence for a distinct behavior of Al^{+2}. In fact, while any pair of species including Al^+, Si^+, and Fe^+ yields correlations with slope unity and low dispersion, pairs including Al^{+2} yield correlations with lower slopes and larger dispersions. One possible explanation of this observational result is that, indeed, Al^{+2} and singly ionized species originate in two different regions. However, the two regions must be physically connected since the velocity profiles of Al^{+2} and low ions are very similar.

We have also identified the existence of an anticorrelation between log $R(Al^{+2}/Al^+)$ and log $N(H^0)$. The anticorrelation appears to be an intrinsic property of DLAs not induced by observational bias, at least as far as the detection limits of Al^+ and Al^{+2} are concerned. We have used such anticorrelation, in conjunction with photoionization equilibrium calculations, to constrain the ionization parameter in DLAs and hence the abundance ionization corrections. We have proposed that low-ionization species in DLAs may arise in two types of regions: (1) an H^0 region opaque to $h\nu > 13.6$ photons and/or (2) a partially ionized, Al^{+2}-bearing interface with small/negligible fractions of high ions such as Si^{+3}. We have considered two types of ionizing continuum: a soft, stellar type ($T_{eff} = 33{,}000$ K) and a hard, QSO-dominated type at $z \approx 2$.

We have successfully reproduced the observed log $R(Al^{+2}/Al^+)$–log $N(H^0)$ anticorrelation by means of a soft-continuum, two-region model (S2 model) with an ionization parameter in the range $10^{-2.6} \lesssim U \lesssim 10^{-1.7}$. In this model most of the neutral hydrogen and low-ionization species originate in the neutral region of type 1. However,

the total hydrogen column density of the partially ionized, type 2 region is relatively high, $3 \times 10^{20}\ \mathrm{cm}^{-2} \lesssim N_2(\mathrm{H}) \lesssim 2 \times 10^{21}\ \mathrm{cm}^{-2}$. At a given value of U, $N_2(\mathrm{H})$ is fixed by the photoionization calculation, and the contribution of the type 2 region decreases as $N(\mathrm{H}^0)$ increases. Because Al^{+2} originates only in the type 2 region, the anticorrelation is naturally explained.

We also tried to reproduce the observed log $R(\mathrm{Al}^{+2}/\mathrm{Al}^{+})$–log $N(\mathrm{H}^0)$ anticorrelation by means of a hard-continuum, one-region model (H1 model). In this model all the species of low- and intermediate-ionization states are assumed to arise in a single layer. In order to reproduce the decrease of log $R(\mathrm{Al}^{+2}/\mathrm{Al}^{+})$ with the correct slope, it is necessary to assume that U must decrease with a law of the type $U \propto N(\mathrm{H}^0)^{-1.5}$. The anticorrelation might be due to the decrease of the mean ionization level with increasing self-shielding by neutral hydrogen. The typical value of the ionization parameter at log $N(\mathrm{H}^0) \simeq 20.8$ is log $U \simeq -4.8$.

We have estimated abundance ionization corrections for 14 elements of astrophysical interest both with the S2 and the H1 model. In both cases, we used the same sets of parameters that allow us to reproduce the anticorrelation between log $R(\mathrm{Al}^{+2}/\mathrm{Al}^{+})$ and log $N(\mathrm{H}^0)$. Ionization corrections can be negative or positive depending on the model adopted and on the species considered. In any case, ionization corrections tend to become smaller in absolute value as $N(\mathrm{H}^0)$ increases.

Ionization corrections are small in both models, but for different reasons. In the S2 model corrections are small because the species used for abundance measurements tend to shift to a higher ionization state in the type 2 region owing to the high value of U that we find. In the H1 model corrections are small because the single region where low-ionization species, together with Al^{+2}, are located has a low level of ionization.

The correction terms for the absolute abundances of N, O, Ti, Cr, Mn, Fe, and Ni are generally below measurement errors ($\approx$0.05/0.1 dex), independent of the adopted ionizing spectrum. Therefore, the deviations from the solar ratio observed in some pairs of iron peak elements, such as the [Mn/Fe] or [Cr/Fe] ratios (Lu et al. 1996; Pettini et al. 2000) are not induced from ionization effects. The Ar/H correction term is negligible for the S2 model but may be significant for the H1 model, in which case the measured $\mathrm{Ar}^0/\mathrm{H}^0$ value would underestimate the intrinsic Ar/H abundance.

The ionization corrections for Mg, Si, P, and S can attain values somewhat higher than the measurement errors. The [N/Si] and [N/S] ratios are modestly affected by ionization effects. As a consequence, the considerable [N/S] and [N/Si] scatter observed at a given metallicity (Centurión et al. 1998; Lu et al. 1998) is a genuine characteristic of DLAs. The [Si/Fe] ratio, a typical indicator of the α/Fe peak ratio, may be overestimated by $\approx$0.1 dex at low $N(\mathrm{H}^0)$ if ionization corrections are not applied. The [S/Zn] ratio might be more sensitive to ionization effects, but the result is uncertain since Zn corrections are probably inaccurate.

The Al corrections can be relatively large. They can be negative or positive, depending whether we adopt the S2 or the H1 model, respectively. The [Al/Fe] and [Al/Si] ratios corrected for dust and ionization effects are below the solar value in the S2 model and somewhat enhanced in the H1 model. These effects, however, are less marked if the Al recombination rate is overestimated.

The Zn corrections are apparently large, but these results may be inaccurate owing to the uncertainties of Zn atomic parameters. From an analysis of [Cr/Zn] and [Fe/Zn] data versus log $N(\mathrm{H}^0)$, we have provided evidence that zinc ionization corrections are likely to be overestimated. Therefore, studies of DLA metallicity based on [Zn/H] data (Pettini et al. 1997; Vladilo et al. 2000) are unlikely to be significantly affected by ionization effects.

We have investigated the stability of the above results in light of possible inaccuracies of Al atomic parameters. In particular, we have considered the possibility, consistent with available data, that the Al^{+} DR rate may be overestimated. We find that in this case, the ionization parameter U and the abundance corrections would be lower both in the S2 and in the H1 model.

The ionization corrections presented here are significantly smaller than the ones predicted by Izotov, Schaerer, & Charbonnel (2001), who have also considered a two-region model of DLA gas. However, these authors assume that the neutral region has much lower metallicity than the ionized one, a strong assumption for which there is little observational support (see Levshakov, Kegel, & Agafonova 2000). With such an assumption, the metal absorptions originate essentially in the ionized region, and the predicted ionization effects are obviously more enhanced than in our case.

Future studies of ionization properties in DLAs would benefit from measurements of ionic ratios other than $\mathrm{Al}^{+2}/\mathrm{Al}^{+}$. One possibility is the $\mathrm{Fe}^{+2}/\mathrm{Fe}^{+}$ ratio given the presence of the 112.2 nm transition of Fe^{+2}, which could be observed in selected cases. From the point of view of the atomic data, it is important to better understand the actual accuracy of atomic parameters and, in particular, those of Al and Zn.

J. C. H. acknowledges support from NASA Long-Term Space Astrophysics grant NAG 5-3485 through Johns Hopkins University. We thank the referee for suggestions that have significantly improved the quality of this work.

APPENDIX A

IONIZATION CORRECTIONS AND IONIZATION RATIOS IN THE TWO-REGION MODEL

We assume that low-ionization species in DLAs arise in two type of regions: (1) an H^0 region completely opaque to ionizing photons with $h\nu > 13.6$ eV and (2) a mildly ionized region containing intermediate-ionization species such as Al^{+2} but not high ions such as C^{3+} or Si^{+3}. The observed column density of the ith ionization state of the element X is given by the relation

$$N(\mathrm{X}^i) = \sum_{k=1,\,2} \int_k x_k(\mathrm{X}^i) A_k(\mathrm{X}) n_k(\mathrm{H}) dl\ , \tag{A1}$$

where $k = 1$ and 2 indicates the neutral and ionized region, respectively, the integrals are carried on along the portions of line of sight l through the two regions, $n_k(\mathrm{X}) = \sum_i n_k(\mathrm{X}^i)$ is the local density (in units of atoms cm^{-3}) of X summed over all the possible ionization states i, $x_k(\mathrm{X}^i) = n_k(X^i)/n_k(X)$ is the ionization fraction of the i-th state, and $A_k(\mathrm{X}) = n_k(\mathrm{X})/n_k(\mathrm{H})$ is the absolute abundance of X.

We assume that type 1 and type 2 regions have equal abundances in a given DLA system: $A_1(\mathrm{X}) = A_2(\mathrm{X}) = A(\mathrm{X})$. For the dominant ionization state in the type 1 region i_d, we have $x_1(\mathrm{X}^{i_d}) = 1$ and, in particular, $x_1(\mathrm{H}^0) = 1$. From these assumptions and from equation (A1), we can express the intrinsic abundance ratio of two elements X and Y in terms of the column density ratio of the dominant species,

$$\frac{A(\mathrm{X})}{A(\mathrm{Y})} = \frac{N(\mathrm{X}^{i_d})}{N(\mathrm{Y}^{i_d})}\,[C(\mathrm{X/Y})]\,, \tag{A2}$$

where

$$C(\mathrm{X/Y}) = \frac{N_1(\mathrm{H}) + \int_2 x_2(\mathrm{Y}^{i_d}) n_2(\mathrm{H}) dl}{N_1(\mathrm{H}) + \int_2 x_2(\mathrm{X}^{i_d}) n_2(\mathrm{H}) dl} \tag{A3}$$

is, by definition, the ionization correction factor and $N_1(\mathrm{H}) = \int_1 n_1(\mathrm{H}) dl$ the mean hydrogen density in the H^0 region. It is easy to obtain similar a expression for the correction term of absolute abundances $C(\mathrm{X/H})$ by replacing Y^{i_d} with H^0 in equation (A3).

We can also derive the column density ratio between two ionization states of a given element. In particular, we are interested in comparing the ionization state that is dominant in the neutral region i_d with higher ionization states i_h. Since $x_1(\mathrm{X}^{i_h}) = 0$ and $x_1(\mathrm{X}^{i_d}) = 1$, we obtain from equation (A1)

$$R(\mathrm{X}^{i_h}/\mathrm{X}^{i_d}) \equiv \frac{N(\mathrm{X}^{i_h})}{N(\mathrm{X}^{i_d})} = \frac{\int_2 x_2(\mathrm{X}^{i_h}) n_2(\mathrm{H}) dl}{N_1(\mathrm{H}) + \int_2 x_2(\mathrm{X}^{i_d}) n_2(\mathrm{H}) dl}\,. \tag{A4}$$

We can derive simpler expressions by introducing the average ionization fractions along the line of sight, $\bar{x}_2(\mathrm{X}^i) = \int_2 x_2(\mathrm{X}^i) n_2(\mathrm{H}) dl / N_2(\mathrm{H})$. With this definition, we obtain

$$C(\mathrm{X/Y}) = \frac{\bar{x}_2(\mathrm{Y}^{i_d}) + N_1/N_2}{\bar{x}_2(\mathrm{X}^{i_d}) + N_1/N_2}\,, \tag{A5}$$

$$C(\mathrm{X/H}) = \frac{\bar{x}_2(\mathrm{H}^0) + N_1/N_2}{\bar{x}_2(\mathrm{X}^{i_d}) + N_1/N_2}\,, \tag{A6}$$

$$R(\mathrm{X}^{i_h}/\mathrm{X}^{i_d}) = \frac{\bar{x}_2(\mathrm{X}^{i_h})}{\bar{x}_2(\mathrm{X}^{i_d}) + N_1/N_2}\,, \tag{A7}$$

where $N_1/N_2 \equiv N_1(\mathrm{H})/N_2(\mathrm{H})$ is the fraction of the line-of-sight total hydrogen column densities in the two regions. The mean ionization fractions $\bar{x}_2(\mathrm{X}^i)$ can be estimated by modeling the intensity and spectrum of the ionizing radiation field in which the clouds are embedded. The parameter N_1/N_2 plays a central role in assessing the importance of ionization effects. When $N_1/N_2 \gg 1$, the ionization corrections are negligible since $C(\mathrm{X/Y}) \simeq 1$ and $C(\mathrm{X/H}) \simeq 1$. In this case, the ionization ratio $R(\mathrm{X}^{i_h}/\mathrm{X}^{i_d})$ tends to be very low no matter what the conditions in the ionized envelope are. On the other hand, if $N_2/N_1 \gg 1$, the ionization corrections and the ionization ratio are representative of the ionized envelope and not of the neutral region. This latter case is appropriate when we consider that all species of low- and intermediate-ionization states originate in a single, partially ionized layer.

REFERENCES

Barker, E. S., Lugger, P. M., Weiler, E. J., & York, D. G. 1984, ApJ, 280, 600
Boissé, P., Le Brun, V., Bergeron, J., & Deharveng, J. M. 1998, A&A, 333, 841
Centurión, M., Bonifacio, P., Molaro, P., & Vladilo, G. 1998, ApJ, 509, 620
———. 2000, ApJ, 536, 540
Dessauges-Zavadsky, M., D'Odorico, S., McMahon, R. G., Molaro, P., Ledoux, C., Peroux, c., & Storrie-Lombardi, L. J. 2001, A&A, 370, 426
D'Odorico, V., & Petitjean, P. 2001, A&A, 370, 729
Ferland, G. J. 1996, HAZY: A Brief Introduction to CLOUDY 90 (Univ. Kentucky Internal Rep.)
Ferland, G. J., Korista, K. T., Verner, D. A., Ferguson, J. W., Kinkgdon, J. B., & Verner, E. M. 1998, PASP, 110, 761
Haardt, F., & Madau, P. 1996, ApJ, 461, 20
Howk, J. C., Savage, B. D., & Fabian, D. 1999, ApJ, 525, 253
Howk, J. C., & Sembach, K. R. 1999, ApJ, 523, L141 (Paper II)
Izotov, Y. I., Schaerer, D., & Charbonnel, C. 2001, ApJ, 549, 878
Izotov, Y. I., & Thuan, T. X. 1999, ApJ, 511, 639
Jenkins, E. B., et al. 2000, ApJ, 538, L81
Kulkarni, V. P., Fall, S. M., & Truran, J. W. 1997, ApJ, 484, L7
Kurucz, R. L. 1991, in Precision Photometry: Astrophysics of the Galaxy, ed. A. C. D. Philip, A. R. Upgren, & K. A. James (Schenectady: Davis), 27
Lauroesch, J. T., Truran, J. W., Welty, D. E., & York, D. G. 1996, PASP, 108, 641
Levshakov, S. A., Kegel, W. H., & Agafonova, I. I. 2001, A&A, 373, 836
Lopez, S., Reimers, D., Rauch, M., Sargent, W. L., & Smette, A. 1999, ApJ, 513, 598
Lu, L., Sargent, W. L. W., & Barlow, T. A. 1996, ApJS, 107, 475
———. 1998, AJ, 115, 55
Lu, L., Savage, B. D., Tripp, T. M., & Meyer, D. 1995, ApJ, 447, 597
Madau, P., Haardt, F., & Rees, M. J. 1999, ApJ, 514, 648
Molaro, P., Bonifacio, P., Centurión, M., D'Odorico, S., Vladilo, G., Santin, P., & Di Marcantonio, P. 2000, ApJ, 541, 54
Nussbaumer, H., & Storey, P. J. 1986, A&AS, 64, 545 (NS86)
Pei, Y. C., Fall, S. M., & Bechtold, J. 1991, ApJ, 378, 6
Pettini, M., Ellison, S. L., Steidel, C. C., Shapley, A. E., & Bowen, D. V. 2000, ApJ, 532, 65
Pettini, M., King, D. L., Smith, L. J., & Hunstead, R. W. 1997, ApJ, 478, 536
Prochaska, J. X., Naumov, S. O., Carney, B. W., McWilliam, A., & Wolfe, A. M. 2000, AJ, 120, 2513
Prochaska, J. X., & Wolfe, A. M. 1996, ApJ, 470, 403
———. 1997, ApJ, 474, 140
———. 1999, ApJS, 121, 369

Savaglio, S., Panagia, N., & Stiavelli, M. 2000, in ASP Conf. Ser. 215, Cosmic Evolution and Galaxy Formation: Structure, Interactions, and Feedback, ed. J. Franco, E. Terlevich, O. López-Cruz, & I. Aretxaga (San Francisco: ASP), 65
Sembach, K. R., Howk, J. C., Ryans, R. S. I., & Keenan, F. P. 2000, ApJ, 528, 310
Sofia, U. J., & Jenkins, E. B. 1998, ApJ, 499, 951
Steidel, C. C., Pettini, M., & Adelberger, K. L. 2001, ApJ, 546, 665
Verner, D. A., Ferland, G. J., Korista, K. T., & Yakovlev, D. G. 1996, ApJ, 465, 487
Viegas, S. M. 1995, MNRAS, 276, 268
Vladilo, G. 1998, ApJ, 493, 583 (Paper I)
Vladilo, G., Bonifacio, P., Centurión, M., & Molaro, P. 2000, ApJ, 543, 24
Wolfe, A. M., Lanzetta, K. M., Foltz, C. B., & Chaffee, F. H. 1995, ApJ, 454, 698
Wolfe, A. M., & Prochaska, J. X. 2000, ApJ, 545, 591